A MoO_3-CoOOH Synergistic Catalyst for Low-Voltage Paired Glycerol Electrolysis

Genxiang Wang[a,b], Pengzhen Zhang[a], Jun Wang[b], Junfeng Wang[a], Xiang Hu[b], Zhiwen Lu[b], Jing Yang*[a, c], Zhenhai Wen*[b], Hao Zhang*[d,e]

a School of Energy and Power Engineering, Jiangsu University, Zhenjiang, 212013, China;

b CAS Key Laboratory of Design and Assembly of Functional Nanostructures, and Fujian Provincial Key Laboratory of Materials and Techniques toward Hydrogen Energy, Fujian Institute of Research on the Structure of Matter, Chinese Academy of Sciences, Fuzhou, Fujian, 350002, China

c Department of Applied Biology and Chemical Technology, The Hong Kong Polytechnic University, Hung Hom, Hong Kong S.A.R, China.

d State Key Laboratory of Chem/Bio-Sensing and Chemometrics, College of Chemistry and Chemical Engineering, Hunan University, Changsha 410082, China.

e Department of Chemical Engineering, Massachusetts Institute of Technology, Cambridge, MA 02139, USA.

EMAIL: hzhchem@mit.edu; wen@fjirsm.ac.cn; jingyang@ujs.edu.cn

Methods

Materials

$Co(NO_3)\cdot 6H_2O$ (AR), and concentrated HNO_3 solution (AR) was purchased from Sinopharm. KOH (AR, 85%) and $(NH_4)_6Mo_7O_{24}.4H_2O$ (RG) were purchased from Adama. Carbon cloth (CC) was bought from Haote New Materials Co. LTD in Jingzhou. HCOOK (99%) and Commercial Pt/C (20%) and Nafion (5%) were bought from Sigma-Aldrich. All the chemical reagents used without further purifying.

Catalyst synthesis

Firstly, the raw carbon cloth was soaked in concentrated HNO_3 solution for 24 h, and then washed with deionized water and dried for electrodeposition. Subsequently, a mixed aqueous solution containing 0.05 M $Co(NO_3)\cdot 6H_2O$ and 5 mM $(NH_4)_6Mo_7O_{24}\cdot 4H_2O$ was prepared as the electrodeposition solution. Then, a three-electrode system was used for electrodeposition with applied electrodeposition potential of -3.1 V *vs.* Ag/AgCl for 500 s at room temperature with the KCl saturated Ag/AgCl as the referenced electrode, carbon cloth (1*1.2 cm^2) as the work electrode and carbon rod as the counter electrode. After the electrodeposition process, the Mo-$Co(OH)_2$ nanosheets supported on CC (MoO_3-$Co(OH)_2$/CC) rinsed with deionized water and dried at 60 °C for use. The controlled samples with single metal compounds ($Co(OH)_2$/CC and MoO_3/CC) were prepared only by changing the electrodeposition solution into 0.05 M $Co(NO_3)\cdot 6H_2O$ aqueous solution and 5 mM $(NH_4)_6Mo_7O_{24}.4H_2O$ aqueous solution, respectively.

Besides, the electrodes with commercial Pt/C (20%) supported on CC with mass loading of 1 mg cm^{-2} were also prepared as the catalyst for hydrogen evolution reaction in cathode. The catalyst ink was prepared by dispersing 5.0 mg catalysts into 500 μL mixture solution of Nafion, isopropanol, deionized water and ethanol with ratio of 2:3:7:8 under ultrasonic agitation at least 0.5 h, then 200 μL of the ink was coated on CC, the Pt/C/CC electrodes were obtained after naturally drying under room temperature.

Materials Characterization

Elemental analysis was conducted using inductively coupled plasma atomic emission spectrometry (ICP-AES, Ultima-2). Powder X-ray diffraction (XRD) patterns were collected at room temperature on a Rigaku Dmax2500 powder X-ray diffractometer using Cu -Kα radiation (λ = 1.540598 Å), scanning a 2θ range from 10 to 70° with a step size of 0.05°. The surface composition and valence states of the catalysts were characterized by X-ray photoelectron spectroscopy (XPS, ESCALAB 250). Morphological and structural features were analyzed using scanning microscopy (SEM, SU-8010) and transmission electron microscopy (TEM, Tecnai F20), with elemental mapping performed via energy-dispersive X-ray spectroscopy (EDS) attached to the TEM. Electrochemical measurements were carried out on a DH 7002D electrochemical workstation (Jiangsu, China). Liquid products were analyzed by 1H nuclear magnetic resonance (^{1}H NMR) spectroscopy on a Bruker AVANCE IIIHD 400 spectrometer. In-situ Raman measurements were conducted using a Horiba Labram HR Evolution Raman system with a 633 nm excitation laser, and the signals were recorded

with a 30-second integration time. The GOR and OER performance over the prepared electrolde was carried out in a custom-made in-situ Raman electrolysis cell filled with 1 M KOH electrolyte with or without 0.5 M glycerol. All applied potentials were referenced to the reversible hydrogen electrode (RHE).

Electrochemical measurement

The electrocatalytic performance of the catalysts toward the GOR was evaluated using a three-electrode system in 1.0 M KOH with or without 0.5 M glycerol on a DH 7002D electrochemical workstation. The working electrode consisted of the prepared electrode, a standard Hg/HgO electrode (1.0 M KOH) served as the reference electrode, and a graphite rod was used as the counter electrode. GOR activities were assessed via linear sweep voltammetry (LSV) at a scan rate of 5 mV s-1. The double-layer capacitance values (C_{dl}) were determined from cyclic voltammetry (CV) curves recorded at scan rates ranging from 20 to 100 mV s^{-1} in increments of 20 mV s-1 within the potential window of 0.826 V to 0.926 V vs. Hg/HgO. Electrochemical impedance spectroscopy (EIS) was conducted at 1.4 V vs. RHE with an AC voltage amplitude of 5 mV over a frequency range of 0.01 Hz to 100 kHz. All potentials were converted to the reversible hydrogen electrode (RHE) scale using the following calibration formula for alkaline electrolyte: E (*vs.* RHE) = E (*vs.* Hg/HgO) + 0.098+ 0.0591* pH.

Electrochemical performance tested in the two-electrode electrolyzer in a home-made flow cell

In the two-electrode electrolyzer configuration, MoO_3-$Co(OH)_2$/CC served as the anode for GOR in 1 M KOH electrolyte with or without 0.5 M glycerol, while

commercial Pt/C/CC acted as the cathode for HER in 0.5 M H_2SO_4 solution. The anode and cathodic compartments were separated by a Nafion 117 membrane. Both electrolytes were continuously circulated using peristaltic pumps. The cell performance was evaluated by linear sweep voltammetry (LSV) with a scan rate of 5 mV s^{-1}.

Explanation of electrochemical neutralization energy (ENE)

In the case of water electrolysis in the alkaline/acid dual-electrolyte electrolyzer:

HER at the cathode:

$$\mathbf{2H^+ + 2e^- \rightarrow H_2} \qquad \textbf{(R1)}$$

$$E_{HER} = E^{\theta}_{H^+/H_2} - 2.303\frac{RT}{2F}\log\left[\frac{\alpha_{H_2}}{(\alpha_{H^+})^2}\right] = 0\ V - 0.059 * pH_{cathode} = 0$$

$$(E^{\theta}_{H^+/H_2} = 0\ V\ vs.\ RHE) \qquad \textbf{(Eq.1)}$$

OER at the anode:

$$\mathbf{4OH^- - 4e^- \rightarrow 2H_2O + O_2} \qquad \textbf{(R2)}$$

$$E_{OER} = E^{\theta}_{O_2/OH^-} - 2.303\frac{RT}{4F}\log\left[\frac{(\alpha_{OH^-})^4}{(\alpha_{H_2O})^2(\alpha_{O_2})}\right] = 1.23\ V - 0.059 * pH_{anode} = 0.404$$

$$(E^{\theta}_{O_2/OH^-} = 1.23\ V\ vs.\ RHE) \qquad \textbf{(Eq.2)}$$

The overall reaction for water splitting:

$$\mathbf{4H^+ + 4OH^- \rightarrow 2H_2O + O_2 + 2H_2} \qquad \textbf{(R3)}$$

$$V_{theoretical\ required} = E^{\theta}_{O_2/OH^-} - E^{\theta}_{H^+/H_2} - 2.303\frac{RT}{4F}\log\left[\frac{(\alpha_{H_2O})^2(\alpha_{O_2})(\alpha_{H_2})^2}{(\alpha_{H^+})^4(\alpha_{OH^-})^4}\right]$$

$$= 1.23 - 0.059 * (pH_{anode} - pH_{cathode}) = \mathbf{0.404} \qquad \textbf{(Eq.3)}$$

In these equations, F is the faraday constant (96 485 C mol^{-1}), T is the room temperature (typically 298.15 K), R is the gas constant (8.314 J mol^{-1} K^{-1}), the term

$pH_{anode} - pH_{cathode}$ denotes the pH difference (ΔpH) between the two chambers. For electrochemical water electrolysis in an alkaline-acid electrolyzer with a ΔpH of 14, the theoretical applied voltage is only 0.404 V, significantly reducing the energy requirement for hydrogen production. Consequently, when the anodic OER is replaced by the glycerol oxidation reaction (GOR), the applied voltage can be further reduced.

Detail of Computational method

Theoretical calculation

Based on combined the performed physical and electrochemical property characterization, we constructed a chemical model for DFT calculations. In this model, a monolayer of CoOOH with a p(3×3) (001) surface, expanded from a single unit cell, was employed as the substrate. This substrate was then combined with a triple-layer MoO_3(001) surface to form a heterostructure, which underwent full structural optimization.

All density functional theory (DFT) calculations were performed using the VASP package (V5.4.4). Structure relaxations and molecular dynamics simulations were carried out using spin-polarized DFT with the Perdew-Burke-Ernzerhof (PBE) functional and a plane-wave basis set with a cutoff energy of 400 eV [4]. Geometry optimizations were performed with convergence criteria of 0.02 eV $Å^{-1}$ for forces and 10^{-5} eV for electronic self-consistent field calculations. The Brillouin zone was sampled using a 2×2×1 Monkhorst-Pack k-point mesh, and van der Waals interactions were addressed by applying the DFT-D3 dispersion correction.[5] All calculations were spin polarized. The gamma point was employed to describe the gas-phase molecules, and a

15 Å^3 cubic lattice was constructed to eliminate interactions between adjacent cells. The DFT+U approach was used to account for on-site Coulomb interactions, with effective U values of 3.0 eV for Co and 5.0 eV for Mo.

The reaction Gibbs free energy (ΔG) was calculated as:

$$\Delta G = \Delta E + \Delta \mathrm{ZPE} - T\Delta S \quad (1)$$

where ΔE is the electric energy difference, ΔZPE is the zero-point energy correction, T is the reaction temperature, and ΔS is the entropy change. The zero-point energy (ZPE) is defined as $\mathrm{ZPE} = \sum_i \frac{1}{2} h\nu_i$, where i is the frequency number, ν_i is the vibrational frequency (in cm^{-1}). The computational hydrogen electrode (CHE) model, developed by Nørskov's group, was used to calculate the free energies of the intermediates involved in the electrochemical reactions [6, 7]. By referencing the standard hydrogen electrode (SHE), we established a connection between the chemical potential of the proton−electron pair ($H^+ + e^-$) and that of ½ H_2, as shown in equation (2):

$$H^+ + e^- \rightarrow \frac{1}{2} H_2 \quad (2)$$

Under standard conditions (pH = 0 in the electrolyte, 1 bar H_2, 298 K), the reaction free energy for the process in equations (3) is equivalent to equations (4):

$$A + H^+ + e^- \rightarrow AH \quad (3)$$

$$\Delta G = G(AH) - G(A) - G\left(H^+ + e^-\right) = G(AH) - G(A) - \frac{1}{2} G(H_2) \quad (4)$$

Where A represents the reactant or intermediates. The effect of electrode bias on steps involving electron transfer was not considered, as all such steps were referenced

to an electrode potential of U = 0 V_{SHE}. This bias shifted the energy of this state by − eU.

We use the mechanism given in Ref. [8] which shows that GOR will go through:

(1)$C_3H_8O_3 + * + 2OH^- \rightarrow *C_3H_6O_3 + 2H_2O + 2e^-$ (R1)

(2)$*C_3H_6O_3 + 3OH^- \rightarrow *C_3H_5O_4^- + 2H_2O + 2e^-$ (R2)

(3)$*C_3H_5O_4^- + 3OH^- \rightarrow *C_2H_3O_3^- + HCOO^- + 2H_2O + 2e^-$ (R3)

(4)$*C_2H_3O_3^- + 3OH^- \rightarrow 2HCOO^- + 2H_2O + * + 2e^-$ (R4)

where * is the active site of catalyst, $*C_3H_6O_3$, $*C_3H_5O_4^-$, $*C_2H_3O_3^-$ are the associated adsorbates of GOR. DFT calculations were used to calculate the standard Gibbs free energy change in all of steps to identify the rate-determining step (RDS) in GOR process. As shown in free energy diagram (**Figure 3e**), the rate-determining step (RDS) is the step of glycerol ($C_3H_8O_3$) to adsorbed-glyceraldehyde ($*C_3H_6O_3$).

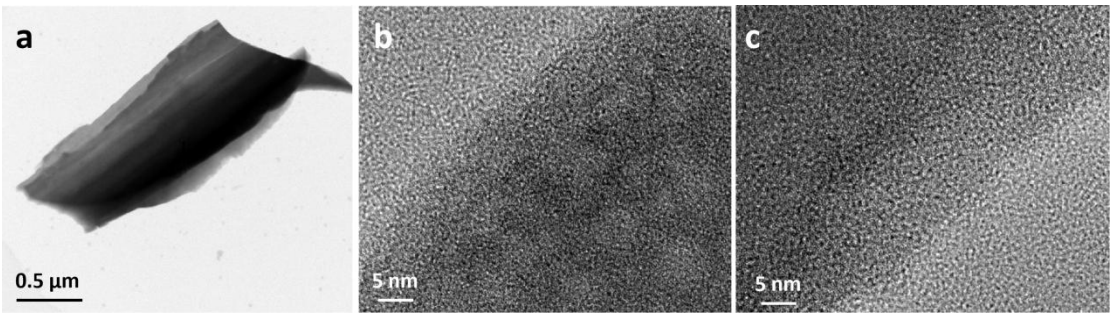

Figure S1. TEM and HRTEM images of MoO_3

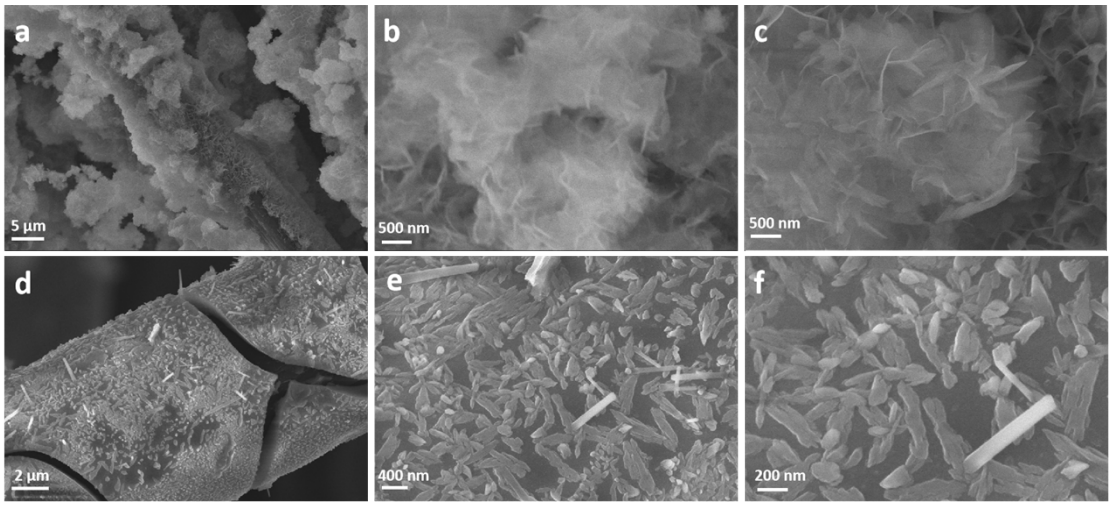

Figure S2. SEM images of $Co(OH)_2$/CC (a-c) and MoO_3/CC (d-e).

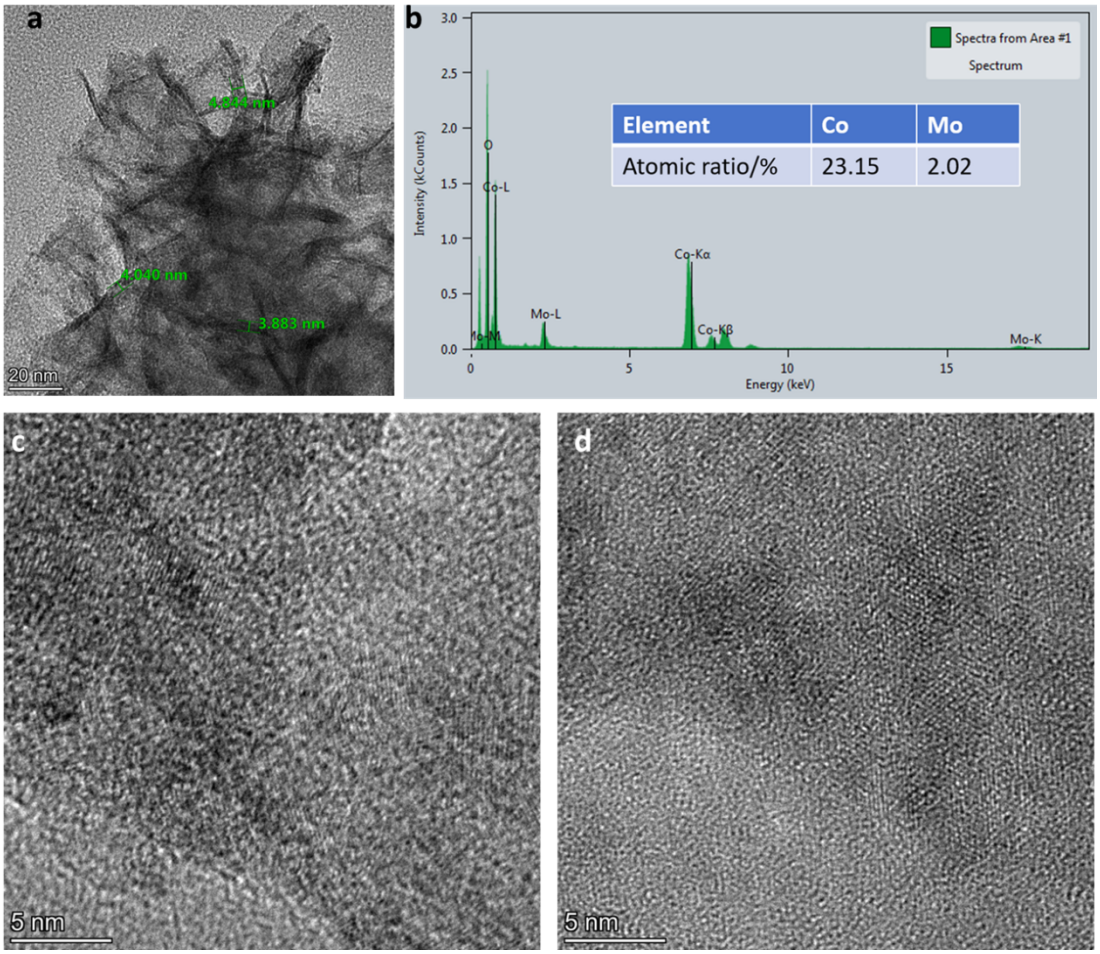

Figure S3. (a) The TEM image of MoO_3-$Co(OH)_2$/CC nanosheets, (b) the EDS element spectrum analysis, (c-d) HRTEM images of MoO_3-$Co(OH)_2$/CC nanosheets

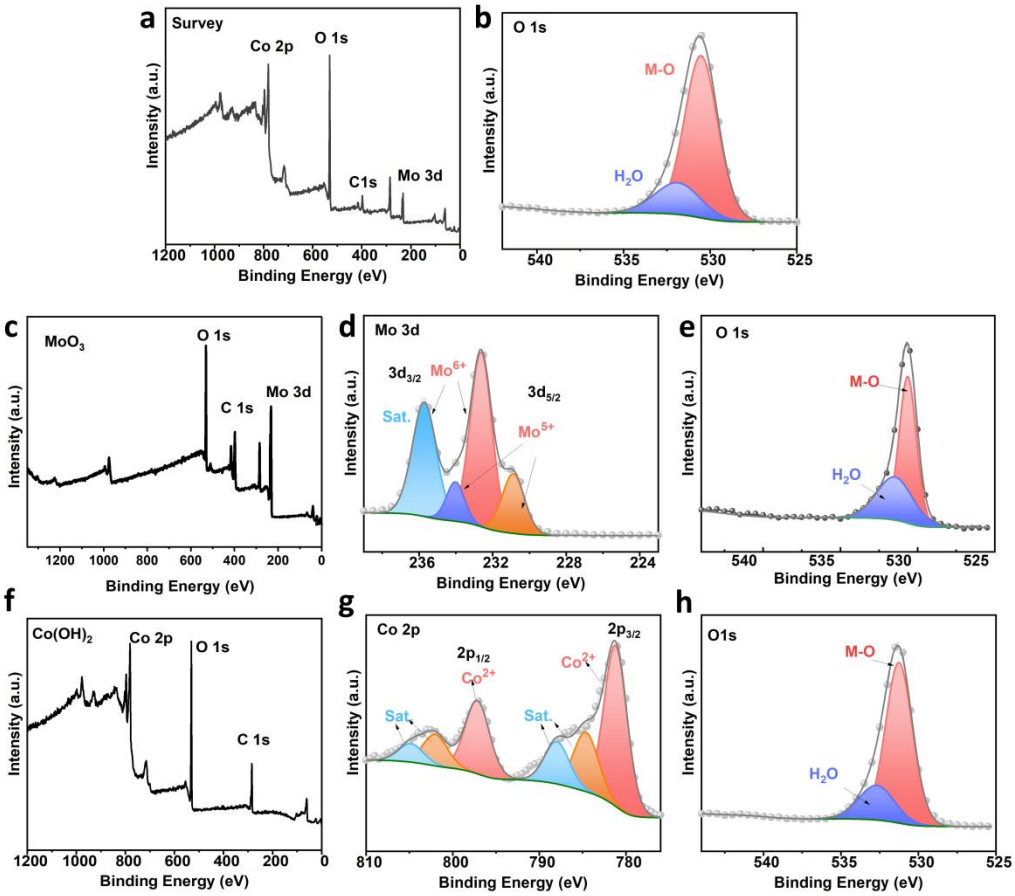

Figure S4. Survey XPS spectra of MoO_3-$Co(OH)_2$/CC (a), MoO_3/CC (c) and $Co(OH)_2$/CC (f), high-resolution XPS spectra of O1s (b) in MoO_3-$Co(OH)_2$/CC Mo 3d (d) and O1s (e) in MoO_3/CC, and Co 2p (g) and O 1s (h) in $Co(OH)_2$/CC.

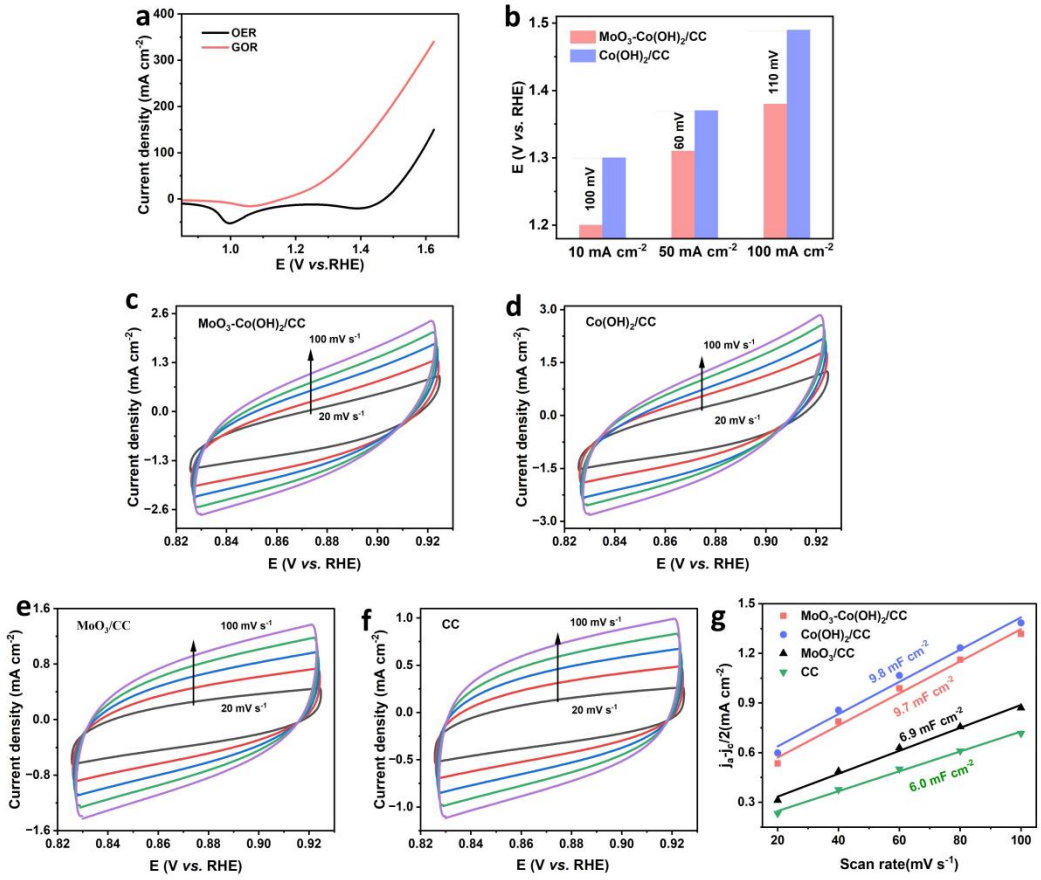

Figure S5. (a) LSV curves GOR and OER over MoO_3-$Co(OH)_2$/CC, (b) comparison of potential at different current densities for GOR, CV curves scanned at different scan rate in the potential range of 0.826 to 0.926 *vs.* Hg/HgO for MoO_3-$Co(OH)_2$/CC (c), $Co(OH)_2$/CC (d), MoO_3 (e) and carbon cloth (CC) (f), C_{dl} values of various catalysts (g)

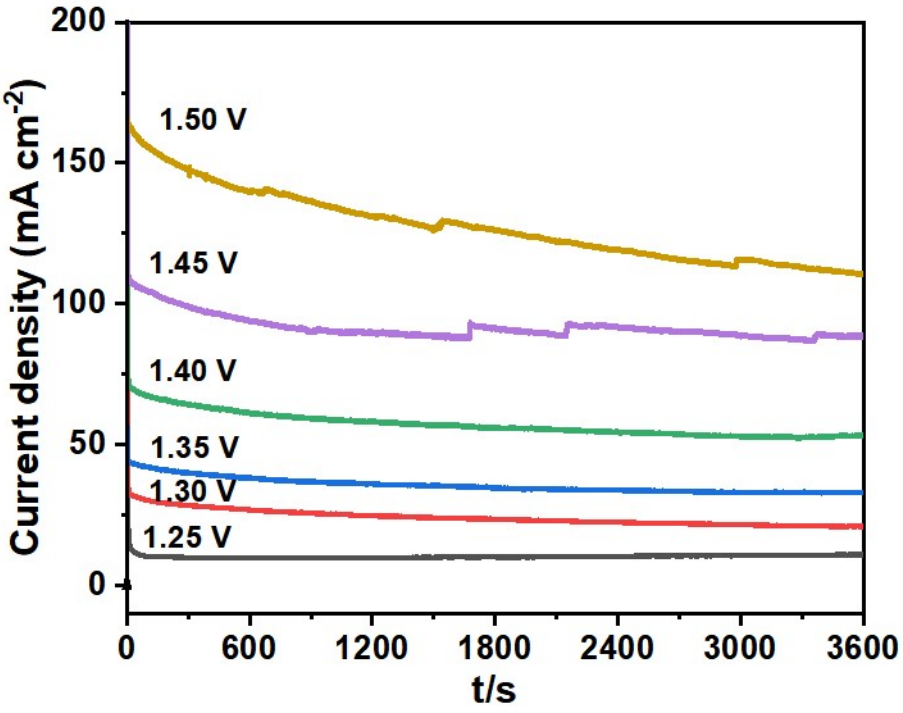

Figure S6. Chronoamperometric response of MoO_3-$Co(OH)_2$/CC at different applied potential in 1.0 M KOH electrolyte containing 0.5 M glycerol

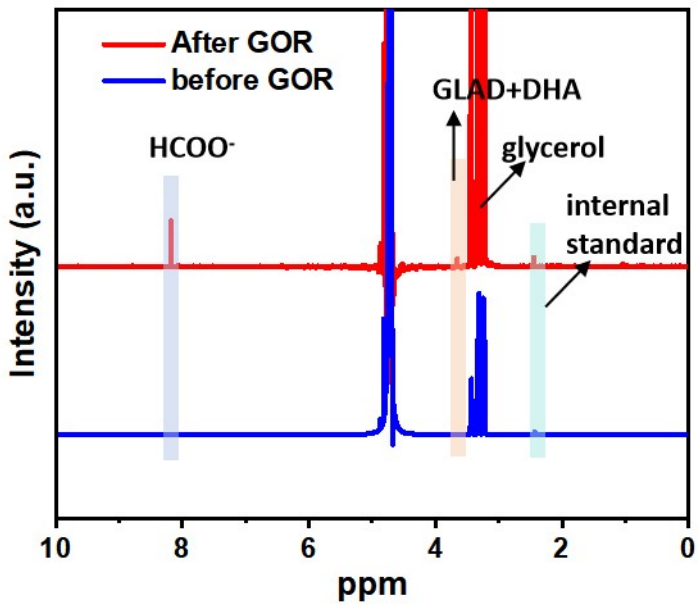

Figure S7. ^{1}H NMR spectra for products before GOR and after GOR by using DMSO as the internal standard

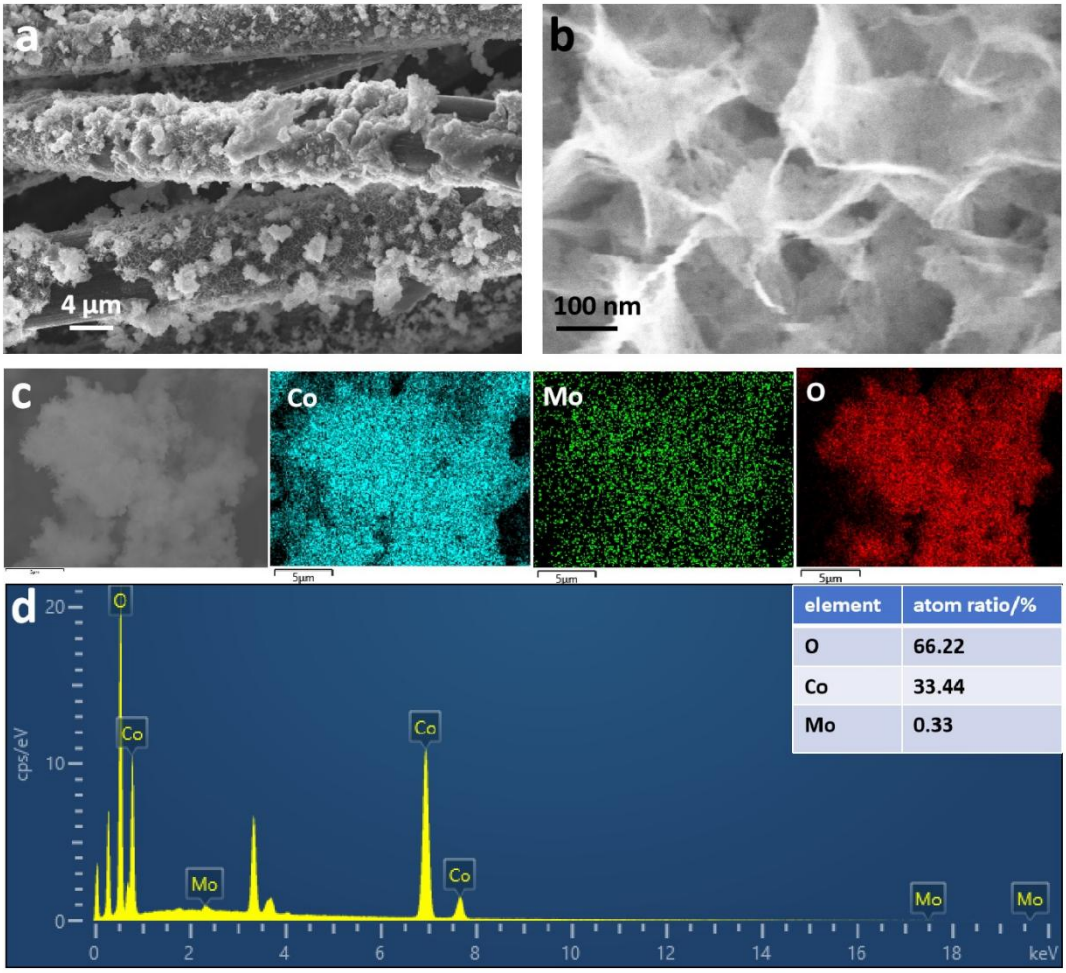

Figure S8. SEM images after GOR (a-b), corresponding elemental mapping images of MoO_3-$Co(OH)_2$/CC (c-d)

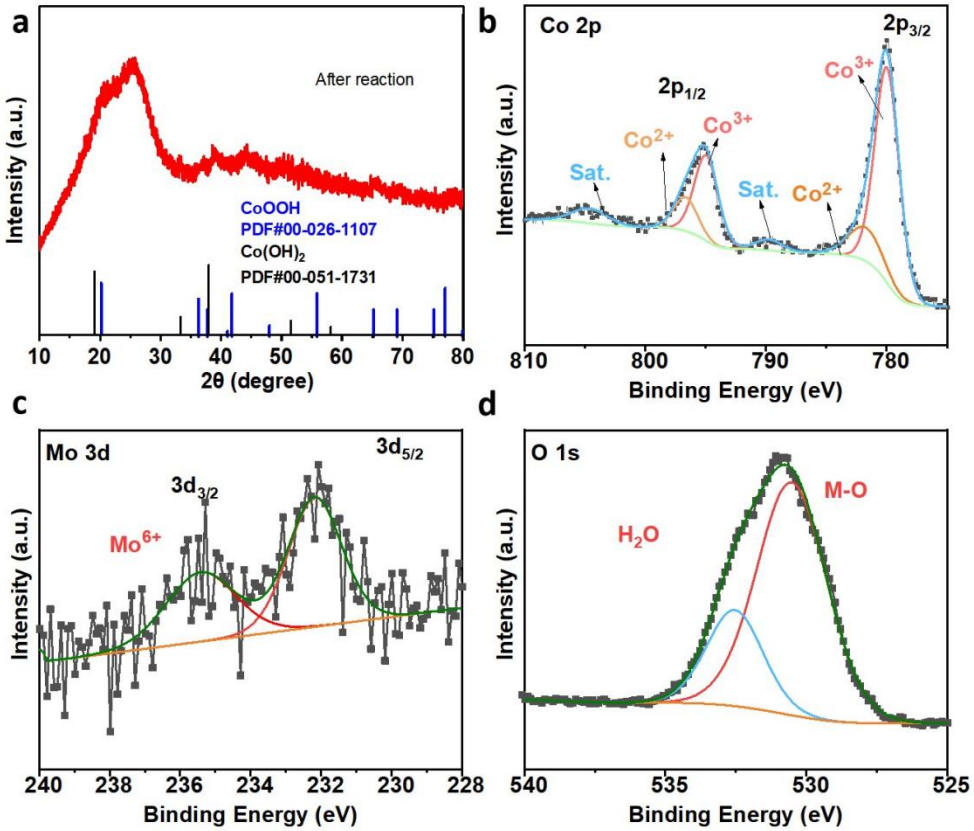

Figure S9. XRD patterns (a), high-resolution Co2p (b), Mo 3d (c), O1s (d) of MoO_3-$Co(OH)_2$/CC after GOR.

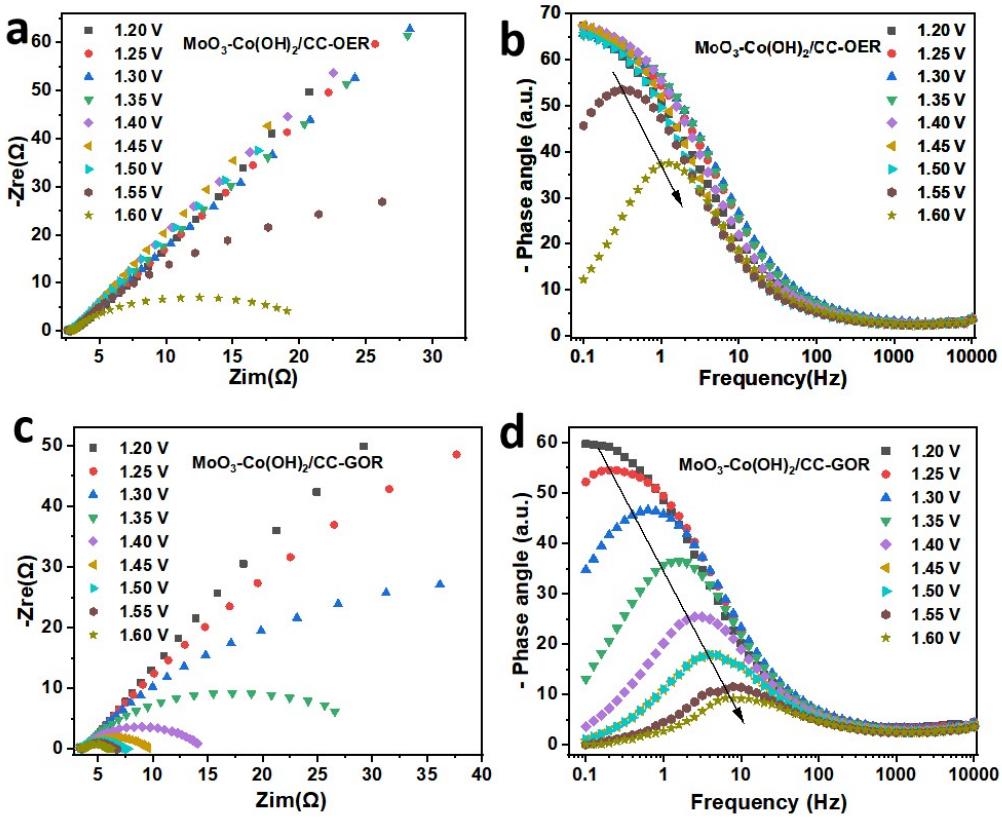

Figure S10. the Nyquist plots (a, c) and Bode plots (b, d) of MoO_3-$Co(OH)_2$/CC with and without 0.5 M glycerol.

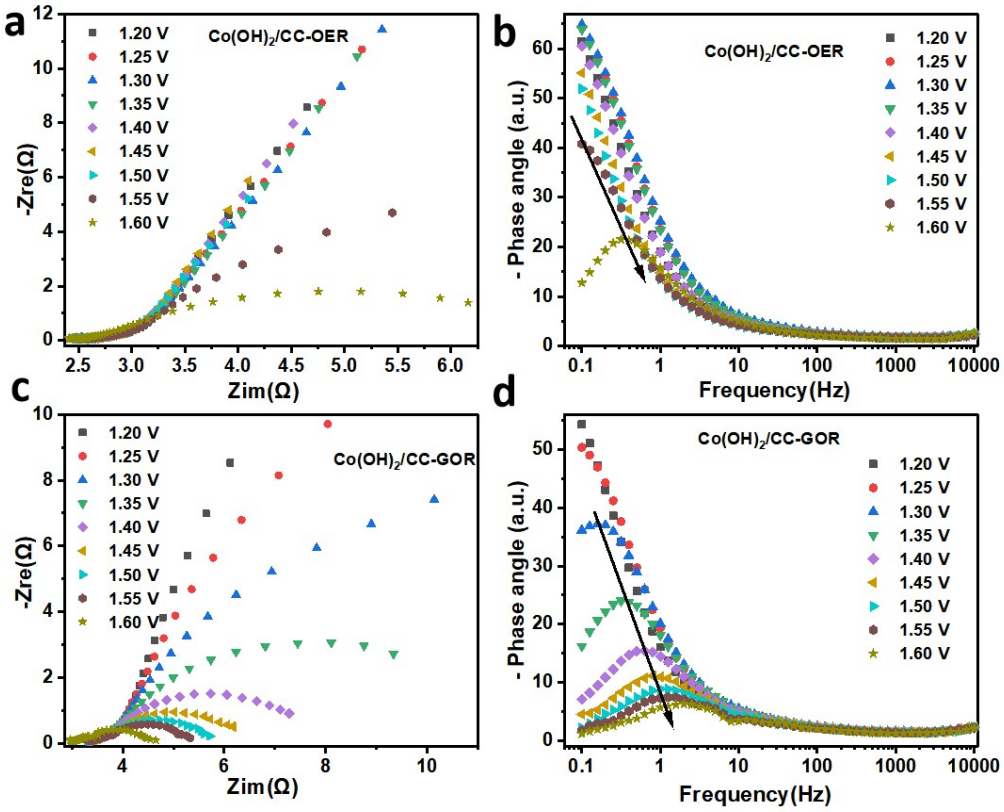

Figure S11. the Nyquist plots (a, c) and Bode plots (b, d) of $Co(OH)_2$/CC and without 0.5 M glycerol.

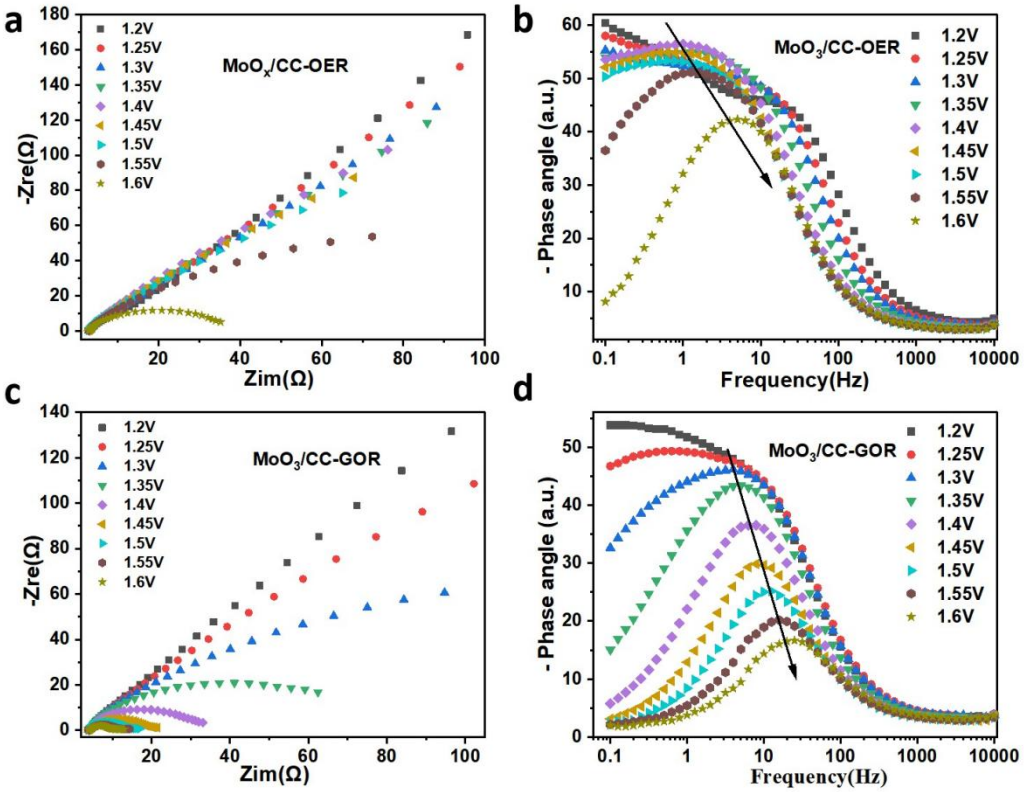

Figure S12. the Nyquist plots (a, c) and Bode plots (b, d) of MoO_3/CC and without 0.5 M glycerol.

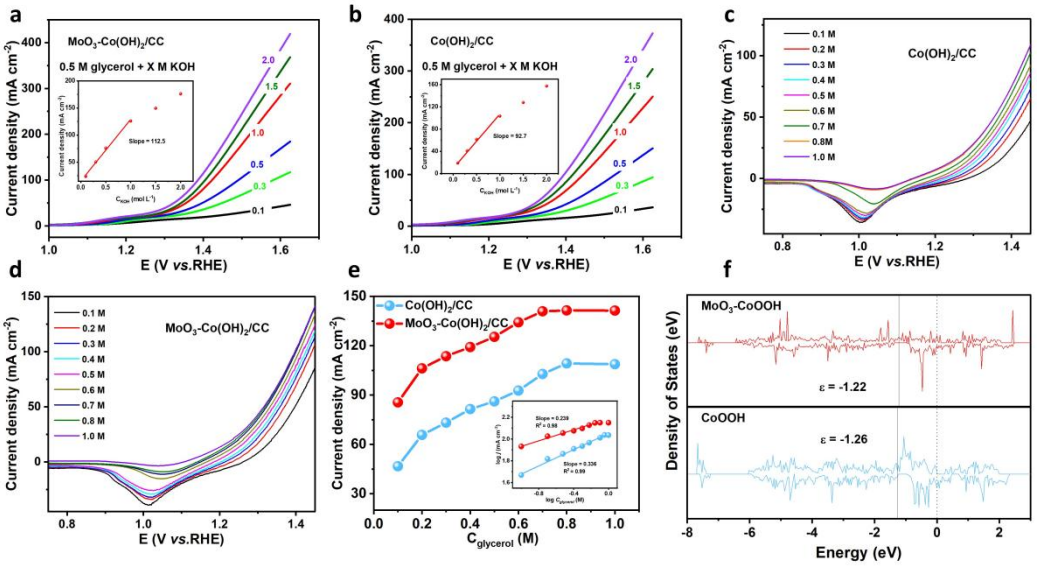

Figure S13. LSV curves measured for MoO_3-$Co(OH)_2$/CC (a) and $Co(OH)_2$/CC (b) in different concentration of KOH with 0.5 M glycerol at a scan rate of 5 mV s^{-1} (inset: the dependence of GOR current density on the KOH concentration at 1.45 V *vs.* RHE), LSV curves measured for $Co(OH)_2$/CC (c) and MoO_3-$Co(OH)_2$/CC (d) in 1M KOH with different glycerol concentration at a scan rate of 5 mV s^{-1}, (e) current densities of $Co(OH)_2$/CC and MoO_3-$Co(OH)_2$/CC at 1.45 V *vs.* RHE in 1 M KOH with different concentrations of glycerol. The inset is the dependence of the GOR on the glycerol concentration at 1.45 V *vs.* RHE (inset: the dependence of GOR current density on the glycerol concentration at 1.45 V vs. RHE). (f) total DOS plots of MoO_3-CoOOH and CoOOH.

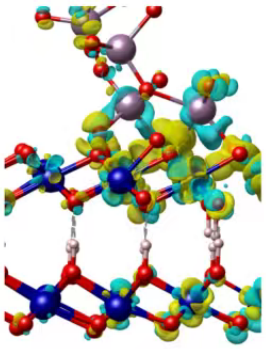

Figure S14. differential charge density of MoO_3-CoOOH. yellow: electron accumulation, blue: electron depletion; isosurface = 0.005 e/Å^3

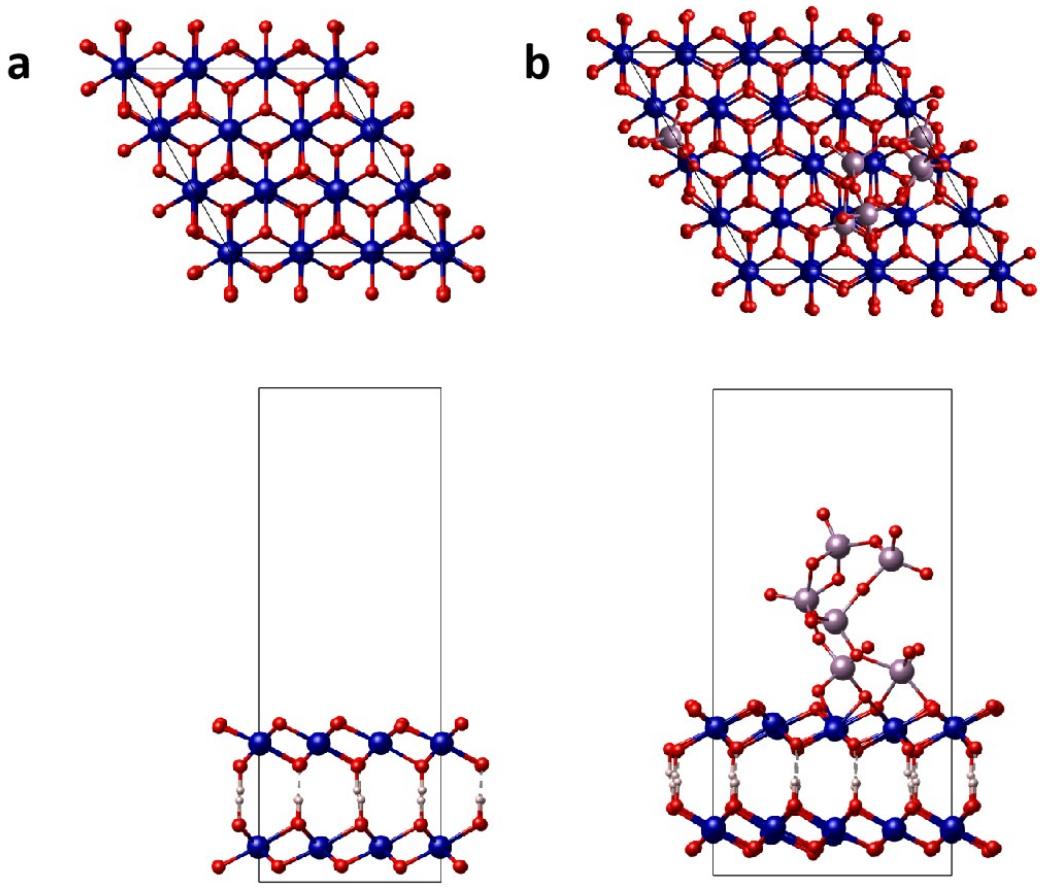

Figure S15. The chemical models of CoOOH (a) and MoO_3-CoOOH for DFT calculations (b)

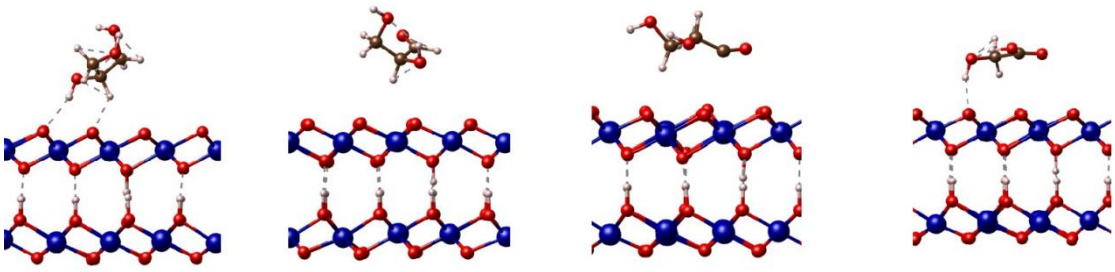

Figure S16. The proposed possible mechanistic pathway of GOR over CoOOH

Table S1. The recent developed Co-based electrocatalysts for GOR

Catalysts	Electrolytes	Potential@current density	Product (Faradic efficiency)	Stability test/h	References
$Co(OH)_2$-SDS	1 M KOH+0.1 M glycerol	1.42@27.73	formate(83.3%)	20	9
$NiCo_2O_4$	1 M KOH+0.1 M glycerol	1.219@10	formate(94%)	/	10
Mn-$CoSe_2$/CFC	1 M KOH+0.1 M glycerol	1.27@10	formate(>90%)	12	11
$CoSe_2$/CC	1 M KOH+0.5 M glycerol	1.23@10	formate(~88%)	90	12
$NiCo_2O_4$	1 M KOH+0.1 M glycerol	1.23@10	formate(~70%)	120	13
Cu-NiCo/NF	1 M KOH+0.1 M glycerol	1.23@10	93.8%(formate)	40	14
Co-Mn-S/NF	1 M KOH+0.1 M glycerol	1.347@100	~90%(formate)	60	15
$CoCuN_{0.6}$/CP	1 M KOH+0.1 M glycerol	1.07@10	90%(formate)	60	16
$NiCo_2O_4$/NF	1 M NaOH+0.1 M glycerol	1.23@10	formate (>97%)	120	17
$CuCo_2O_4$	0.1 M KOH+0.1 M glycerol	1.26 V@10 mA cm^{-2}	formate(80.6%)	19	18
$NiCo_2O_4$/NF	1 M KOH+0.5 M glycerol	1.15@10	formate (91.2%)	12	19
OX-$Ni_{0.5}Co_{0.5}(OH)_2$	1 M KOH+0.1 M glycerol	1.26@10	formate (91.%)	20	20
CoO/NF	1 M KOH+0.1 M glycerol	1.201@10	formate (91.3%)	108	21
$NiCo_2O_4$/NF	1 M KOH+0.1 M glycerol	1.42@300	formate (89.9%), GLA (7.62%)	48	22
MoO_3-$Co(OH)_2$/CC	1 M KOH+0.1 M glycerol	1.20@10	formate (98.2%)	120	This work

References:

1. G. Wang, J. Chen, Y. Li, J. Jia, P. Cai and Z. Wen, *Chem. Commun.*, 2018, **54**, 2603-2606.
2. Y. Ding, P. Cai and Z. Wen, *Chem. Soc. Rev.*, 2021, **50**, 1495-1511.
3. L. Fan, Y. Ji, G. Wang, J. Chen, K. Chen, X. Liu and Z. Wen, *J. Am. Chem. Soc.,* 2022, **144,** 7224-7235.
4. A. E. Mattsson, R. Armiento, P. A. Schultz and T. R. Mattsson, *Phys. Rev. B Condensed Matter Mater. Phys.*, 2006, **73,** 195123.
5. H. Schröder, J. Hühnert and T. Schwabe, *J. Chem. Phys.*, 2017, **146**, 044115.
6. G. T. K. K. Gunasooriya and J. K. Nørskov, *ACS Energy Lett.,* 2020, **5,** 3778-3787.
7. S. R. Kelly, C. Kirk, K. Chan and J. K. Nørskov, *J. Phys. Chem. C,* 2020, **124,** 14581-14591.
8. A. C. Brix, D. M. Morales, M. Braun, D. Jambrec, J. R. C. Junqueira, S. Cychy, S. Seisel, J. Masa, M. Muhler, C. Andronescu and W. Schuhmann, *ChemElectroChem,* 2021, **8**, 2336-2342.
9. L. Li, Z. Zhang, H. Chen and F. Chen, Promoting electrocatalytic alcohols oxidation coupled with H_2 production via ligand intercalation strategy, *Nano Res.* 2022, **16**, 4596-4602.
10. J. Ma, X. Wang, J. Song, Y. Tang, T. Sun, L. Liu, J. Wang, J. Wang and M. Yang, *Angew. Chem. Int. Ed.* 2024, **63**, e202319153.
11. L. Fan, Y. Ji, G. Wang, Z. Zhang, L. Yi, K. Chen, X. Liu and Z. Wen, *J. Energy Chem.,* 2022, **72**, 424-431.
12. G. X. Wang, J. X. Chen, K. K. Li, J. H. Huang, Y. C. Huang, Y. J. Liu, X. Hu, B. S. Zhao, L. C. Yi, T. W. Jones and Z. H. Wen, *Nano Energy*, 2022, **92**, 106751.
13. Y. Duan, M. Xue, B. Liu, M. Zhang, Y. Wang, B. Wang, R. Zhang and K. Yan, *Chin. J. Catal*., 2024, **57**, 68-79.
14. C. Li, H. Li, B. Zhang, H. Li, Y. Wang, X. Wang, P. Das, Y. Li, X. Wu, Y. Li, Y. Cui, J. Xiao and Z. S. Wu, *Angew. Chem. Int. Ed.,* 2024, **63**, 2411542.
15. Y. Fang, C. Dai, X. Liu, Y. Wang, C. Ju, S. He, R. Shi, Y. Liu, J. Zhang, Y. Zhu

and J. Wang, *Nano Energy*, 2024, **127**, 109754.

16. K. Shi, D. Si, X. Teng, L. Chen and J. Shi, *Chin. J Catal*., 2023, **53**, 143-152.
17. G. Wu, X. Dong, J. Mao, G. Li, C. Zhu, S. Li, A. Chen, G. Feng, Y. Song, W. Chen and W. Wei, *Chem. Eng. J*., 2023, **468**, 143640.
18. X. T. Han, H. Y. Sheng, C. Yu, T. W. Walker, G. W. Huber, J. S. Qiu and S. Jin, *ACS Catal.,* 2020, **10**, 6741-6752.
19. X. Feng, K. Guo, C. Jia, B. Liu, S. Ci, J. Chen and Z. Wen, *Acta Phys. Chim. Sin.*, 2023, **0**, 2303050.
20. Y. Zou, W. D. Zhang, H. Xu, J. Yang, J. Liu, Z. G. Gu and X. Yan, *J. Colloid Interface Sci*., 2023, **650**, 701-709.
21. H. Ren, Z. Huang, G. Cai, J. Guo, Y. Sun, W. Yao, D. Ye, H. Qian, J. Zhang and H. Zhao, *J. Alloy Compd*., 2024, **996**.
22. W. Luo, H. Tian, Q. Li, G. Meng, Z. Chang, C. Chen, R. Shen, X. Yu, L. Zhu, F. Kong, X. Cui and J. Shi, *Adv. Funct. Mater*., 2023, **34**, 2306995.